

Forward Neutral Pion Transverse Single Spin Asymmetries in p+p Collisions at $\sqrt{s} = 200$ GeV

B.I. Abelev,¹⁰ M.M. Aggarwal,³² Z. Ahammed,⁴⁷ B.D. Anderson,²¹ D. Arkhipkin,¹⁴ G.S. Averichev,¹³ Y. Bai,³⁰ J. Balewski,¹⁸ O. Barannikova,¹⁰ L.S. Barnby,² J. Baudot,¹⁹ S. Baumgart,⁵² D.R. Beavis,³ R. Bellwied,⁵⁰ F. Benedosso,³⁰ R.R. Betts,¹⁰ S. Bhardwaj,³⁷ A. Bhasin,²⁰ A.K. Bhati,³² H. Bichsel,⁴⁹ J. Bielcik,¹² J. Bielcikova,¹² L.C. Bland,³ S-L. Blyth,²⁴ M. Bombara,² B.E. Bonner,³⁸ M. Botje,³⁰ J. Bouchet,⁴² E. Braidot,³⁰ A.V. Brandin,²⁸ S. Bueltmann,³ T.P. Burton,² M. Bystersky,¹² X.Z. Cai,⁴¹ H. Caines,⁵² M. Calderón de la Barca Sánchez,⁶ J. Callner,¹⁰ O. Catu,⁵² D. Cebra,⁶ M.C. Cervantes,⁴³ Z. Chajecski,³¹ P. Chaloupka,¹² S. Chattopadhyay,⁴⁷ H.F. Chen,⁴⁰ J.H. Chen,⁴¹ J.Y. Chen,⁵¹ J. Cheng,⁴⁵ M. Cherney,¹¹ A. Chikanian,⁵² K.E. Choi,³⁶ W. Christie,³ S.U. Chung,³ R.F. Clarke,⁴³ M.J.M. Coddington,⁴³ J.P. Coffin,¹⁹ T.M. Cormier,⁵⁰ M.R. Cosentino,³⁹ J.G. Cramer,⁴⁹ H.J. Crawford,⁵ D. Das,⁶ S. Dash,¹⁶ M. Daugherty,⁴⁴ M.M. de Moura,³⁹ T.G. Dedovich,¹³ M. DePhillips,³ A.A. Derevschikov,³⁴ R. Derradi de Souza,⁸ L. Didenko,³ T. Dietel,¹⁵ P. Djawotho,¹⁸ S.M. Dogra,²⁰ X. Dong,²⁴ J.L. Drachenberg,⁴³ J.E. Draper,⁶ F. Du,⁵² J.C. Dunlop,³ M.R. Dutta Mazumdar,⁴⁷ W.R. Edwards,²⁴ L.G. Efimov,¹³ E. Elhalhuli,² V. Emelianov,²⁸ J. Engelage,⁵ G. Eppley,³⁸ B. Erazmus,⁴² M. Estienne,¹⁹ L. Eun,³³ P. Fachini,³ R. Fatemi,²² J. Fedorisin,¹³ A. Feng,⁵¹ P. Filip,¹⁴ E. Finch,⁵² V. Fine,³ Y. Fisyak,³ J. Fu,⁵¹ C.A. Gagliardi,⁴³ L. Gaillard,² M.S. Ganti,⁴⁷ E. Garcia-Solis,¹⁰ V. Ghazikhanian,⁷ P. Ghosh,⁴⁷ Y.N. Gorbunov,¹¹ A. Gordon,³ H. Gos,⁴⁸ O. Grebenyuk,³⁰ D. Grosnick,⁴⁶ B. Grube,³⁶ S.M. Guertin,⁷ K.S.F.F. Guimaraes,³⁹ A. Gupta,²⁰ N. Gupta,²⁰ W. Guryn,³ B. Haag,⁶ T.J. Hallman,³ A. Hamed,⁴³ J.W. Harris,⁵² W. He,¹⁸ M. Heinz,⁵² T.W. Henry,⁴³ S. Heppelmann,³³ B. Hippolyte,¹⁹ A. Hirsch,³⁵ E. Hjort,²⁴ A.M. Hoffman,²⁵ G.W. Hoffmann,⁴⁴ D.J. Hofman,¹⁰ R.S. Hollis,¹⁰ M.J. Horner,²⁴ H.Z. Huang,⁷ E.W. Hughes,⁴ T.J. Humanic,³¹ G. Igo,⁷ A. Iordanova,¹⁰ P. Jacobs,²⁴ W.W. Jacobs,¹⁸ P. Jakl,¹² F. Jin,⁴¹ P.G. Jones,² E.G. Judd,⁵ S. Kabana,⁴² K. Kajimoto,⁴⁴ K. Kang,⁴⁵ J. Kapitan,¹² M. Kaplan,⁹ D. Keane,²¹ A. Kechechyan,¹³ D. Kettler,⁴⁹ V.Yu. Khodyrev,³⁴ J. Kiryluk,²⁴ A. Kisiel,³¹ S.R. Klein,²⁴ A.G. Knospe,⁵² A. Kocoloski,²⁵ D.D. Koetke,⁴⁶ T. Kollegger,¹⁵ M. Kopytine,²¹ L. Kotchenda,²⁸ V. Kouchpil,¹² K.L. Kowalik,²⁴ P. Kravtsov,²⁸ V.I. Kravtsov,³⁴ K. Krueger,¹ C. Kuhn,¹⁹ A. Kumar,³² P. Kurnadi,⁷ M.A.C. Lamont,³ J.M. Landgraf,³ J. Langdon,³ S. Lange,¹⁵ S. LaPointe,⁵⁰ F. Laue,³ J. Lauret,³ A. Lebedev,³ R. Lednicky,¹⁴ C-H. Lee,³⁶ M.J. LeVine,³ C. Li,⁴⁰ Q. Li,⁵⁰ Y. Li,⁴⁵ G. Lin,⁵² X. Lin,⁵¹ S.J. Lindenbaum,²⁹ M.A. Lisa,³¹ F. Liu,⁵¹ H. Liu,⁴⁰ J. Liu,³⁸ L. Liu,⁵¹ T. Ljubicic,³ W.J. Llope,³⁸ R.S. Longacre,³ W.A. Love,³ Y. Lu,⁴⁰ T. Ludlam,³ D. Lynn,³ G.L. Ma,⁴¹ J.G. Ma,⁷ Y.G. Ma,⁴¹ D.P. Mahapatra,¹⁶ R. Majka,⁵² L.K. Mangotra,²⁰ R. Manweiler,⁴⁶ S. Margetis,²¹ C. Markert,⁴⁴ H.S. Matis,²⁴ Yu.A. Matulenko,³⁴ T.S. McShane,¹¹ A. Meschanin,³⁴ J. Millane,²⁵ C. Miller,³ M.L. Miller,²⁵ N.G. Minaev,³⁴ S. Mioduszewski,⁴³ A. Mischke,³⁰ J. Mitchell,³⁸ B. Mohanty,⁴⁷ D.A. Morozov,³⁴ M.G. Munhoz,³⁹ B.K. Nandi,¹⁷ C. Nattrass,⁵² T.K. Nayak,⁴⁷ J.M. Nelson,² C. Nepali,²¹ P.K. Netrakanti,³⁵ M.J. Ng,⁵ L.V. Nogach,³⁴ S.B. Nurushev,³⁴ G. Odyniec,²⁴ A. Ogawa,³ H. Okada,³ V. Okorokov,²⁸ D. Olson,²⁴ M. Pachr,¹² S.K. Pal,⁴⁷ Y. Panebratsev,¹³ A.I. Pavlinov,⁵⁰ T. Pawlak,⁴⁸ T. Peitzmann,³⁰ V. Perevoztchikov,³ C. Perkins,⁵ W. Peryt,⁴⁸ S.C. Phatak,¹⁶ M. Planinic,⁵³ J. Pluta,⁴⁸ N. Poljak,⁵³ N. Porile,³⁵ A.M. Poskanzer,²⁴ M. Potekhin,³ B.V.K.S. Potukuchi,²⁰ D. Prindle,⁴⁹ C. Pruneau,⁵⁰ N.K. Pruthi,³² J. Putschke,⁵² I.A. Qattan,¹⁸ G. Rakness,^{3,33} R. Raniwala,³⁷ S. Raniwala,³⁷ R.L. Ray,⁴⁴ D. Relyea,⁴ A. Ridiger,²⁸ H.G. Ritter,²⁴ J.B. Roberts,³⁸ O.V. Rogachevskiy,¹³ J.L. Romero,⁶ A. Rose,²⁴ C. Roy,⁴² L. Ruan,³ M.J. Russcher,³⁰ V. Rykov,²¹ R. Sahoo,⁴² I. Sakrejda,²⁴ T. Sakuma,²⁵ S. Salur,⁵² J. Sandweiss,⁵² M. Sarsour,⁴³ J. Schambach,⁴⁴ R.P. Scharenberg,³⁵ N. Schmitz,²⁶ J. Seger,¹¹ I. Selyuzhenkov,⁵⁰ P. Seyboth,²⁶ A. Shabetai,¹⁹ E. Shahaliev,¹³ M. Shao,⁴⁰ M. Sharma,³² X-H. Shi,⁴¹ E.P. Sichtermann,²⁴ F. Simon,²⁶ R.N. Singaraju,⁴⁷ M.J. Skoby,³⁵ N. Smirnov,⁵² R. Snellings,³⁰ P. Sorensen,³ J. Sowinski,¹⁸ J. Speltz,¹⁹ H.M. Spinka,¹ B. Srivastava,³⁵ A. Stadnik,¹³ T.D.S. Stanislaus,⁴⁶ D. Staszak,⁷ R. Stock,¹⁵ M. Strikhanov,²⁸ B. Stringfellow,³⁵ A.A.P. Suaide,³⁹ M.C. Suarez,¹⁰ N.L. Subba,²¹ M. Sumner,¹² X.M. Sun,²⁴ Z. Sun,²³ B. Surrow,²⁵ T.J.M. Symons,²⁴ A. Szanto de Toledo,³⁹ J. Takahashi,⁸ A.H. Tang,³ Z. Tang,⁴⁰ T. Tarnowsky,³⁵ J. Tatarowicz,³³ D. Thein,⁴⁴ J.H. Thomas,²⁴ J. Tian,⁴¹ A.R. Timmins,² S. Timoshenko,²⁸ M. Tokarev,¹³ T.A. Trainor,⁴⁹ V.N. Tram,²⁴ A.L. Trattner,⁵ S. Trentalange,⁷ R.E. Tribble,⁴³ O.D. Tsai,⁷ J. Ulery,³⁵ T. Ullrich,³ D.G. Underwood,¹ G. Van Buren,³ N. van der Kolk,³⁰ M. van Leeuwen,²⁴ A.M. Vander Molen,²⁷ R. Varma,¹⁷ G.M.S. Vasconcelos,⁸ I.M. Vasilevski,¹⁴ A.N. Vasiliev,³⁴ R. Vernet,¹⁹ F. Videbaek,³ S.E. Vigdor,¹⁸ Y.P. Viyogi,¹⁶ S. Vokal,¹³ S.A. Voloshin,⁵⁰ M. Wada,⁴⁴ W.T. Waggoner,¹¹ F. Wang,³⁵ G. Wang,⁷ J.S. Wang,²³ Q. Wang,³⁵ X. Wang,⁴⁵ X.L. Wang,⁴⁰ Y. Wang,⁴⁵ J.C. Webb,⁴⁶ G.D. Westfall,²⁷ C. Whitten Jr.,⁷ H. Wieman,²⁴ S.W. Wissink,¹⁸ R. Witt,⁵² J. Wu,⁴⁰ Y. Wu,⁵¹ N. Xu,²⁴ Q.H. Xu,²⁴ Z. Xu,³

P. Yepes,³⁸ I-K. Yoo,³⁶ Q. Yue,⁴⁵ N. Zachariou,³ M. Zawisza,⁴⁸ W. Zhan,²³ H. Zhang,³ S. Zhang,⁴¹ W.M. Zhang,²¹ Y. Zhang,⁴⁰ Z.P. Zhang,⁴⁰ Y. Zhao,⁴⁰ C. Zhong,⁴¹ J. Zhou,³⁸ R. Zoukarneev,¹⁴ Y. Zoukarneeva,¹⁴ and J.X. Zuo⁴¹
(STAR Collaboration),*

- ¹Argonne National Laboratory, Argonne, Illinois 60439
²University of Birmingham, Birmingham, United Kingdom
³Brookhaven National Laboratory, Upton, New York 11973
⁴California Institute of Technology, Pasadena, California 91125
⁵University of California, Berkeley, California 94720
⁶University of California, Davis, California 95616
⁷University of California, Los Angeles, California 90095
⁸Universidade Estadual de Campinas, Sao Paulo, Brazil
⁹Carnegie Mellon University, Pittsburgh, Pennsylvania 15213
¹⁰University of Illinois at Chicago, Chicago, Illinois 60607
¹¹Creighton University, Omaha, Nebraska 68178
¹²Nuclear Physics Institute AS CR, 250 68 Řež/Prague, Czech Republic
¹³Laboratory for High Energy (JINR), Dubna, Russia
¹⁴Particle Physics Laboratory (JINR), Dubna, Russia
¹⁵University of Frankfurt, Frankfurt, Germany
¹⁶Institute of Physics, Bhubaneswar 751005, India
¹⁷Indian Institute of Technology, Mumbai, India
¹⁸Indiana University, Bloomington, Indiana 47408
¹⁹Institut de Recherches Subatomiques, Strasbourg, France
²⁰University of Jammu, Jammu 180001, India
²¹Kent State University, Kent, Ohio 44242
²²University of Kentucky, Lexington, Kentucky, 40506-0055
²³Institute of Modern Physics, Lanzhou, China
²⁴Lawrence Berkeley National Laboratory, Berkeley, California 94720
²⁵Massachusetts Institute of Technology, Cambridge, MA 02139-4307
²⁶Max-Planck-Institut für Physik, Munich, Germany
²⁷Michigan State University, East Lansing, Michigan 48824
²⁸Moscow Engineering Physics Institute, Moscow Russia
²⁹City College of New York, New York City, New York 10031
³⁰NIKHEF and Utrecht University, Amsterdam, The Netherlands
³¹Ohio State University, Columbus, Ohio 43210
³²Panjab University, Chandigarh 160014, India
³³Pennsylvania State University, University Park, Pennsylvania 16802
³⁴Institute of High Energy Physics, Protvino, Russia
³⁵Purdue University, West Lafayette, Indiana 47907
³⁶Pusan National University, Pusan, Republic of Korea
³⁷University of Rajasthan, Jaipur 302004, India
³⁸Rice University, Houston, Texas 77251
³⁹Universidade de Sao Paulo, Sao Paulo, Brazil
⁴⁰University of Science & Technology of China, Hefei 230026, China
⁴¹Shanghai Institute of Applied Physics, Shanghai 201800, China
⁴²SUBATECH, Nantes, France
⁴³Texas A&M University, College Station, Texas 77843
⁴⁴University of Texas, Austin, Texas 78712
⁴⁵Tsinghua University, Beijing 100084, China
⁴⁶Valparaiso University, Valparaiso, Indiana 46383
⁴⁷Variable Energy Cyclotron Centre, Kolkata 700064, India
⁴⁸Warsaw University of Technology, Warsaw, Poland
⁴⁹University of Washington, Seattle, Washington 98195
⁵⁰Wayne State University, Detroit, Michigan 48201
⁵¹Institute of Particle Physics, CCNU (HZNU), Wuhan 430079, China
⁵²Yale University, New Haven, Connecticut 06520
⁵³University of Zagreb, Zagreb, HR-10002, Croatia

(Dated: October 25, 2018)

We report precision measurements of the Feynman- x (x_F) dependence, and first measurements of the transverse momentum (p_T) dependence, of transverse single spin asymmetries for the production of π^0 mesons from polarized proton collisions at $\sqrt{s}=200$ GeV. The x_F dependence of the results are in fair agreement with perturbative QCD (pQCD) model calculations that identify orbital motion of

quarks and gluons within the proton as the origin of the spin effects. Results for the p_T dependence at fixed x_F are not consistent with these same pQCD-based calculations.

PACS numbers:

The production of particles with high transverse momentum from polarized proton collisions at high energies is sensitive to the quark (q) and gluon (g) spin structure of the proton. Perturbative QCD (pQCD) calculations are used to interpret spin observables when they can explain measured cross sections. The goal of measuring spin observables is to understand how the proton gets its spin from its q, g constituents.

One challenge to theory has been to understand the azimuthal asymmetry of particles produced in collisions of transversely polarized protons, known as analyzing power (A_N) or transverse single spin asymmetry. With vertical polarization, non-zero A_N corresponds to a left-right asymmetry of the produced particles. Sizeable A_N are not expected in collinear pQCD at leading twist due to the chiral properties of the theory [1]. Nonetheless, large A_N are observed for inclusive pion production in $p_\uparrow + p$ collisions over a broad range of collision energies (\sqrt{s}) [2, 3, 4, 5, 6] and in semi-inclusive deep inelastic scattering (SIDIS) from transversely polarized proton targets [7]. These observations have prompted extensions to pQCD that introduce transverse momentum dependence (TMD) correlated with the spin degree of freedom. For example, A_N could be generated by spin-correlated TMD fragmentation if there is transverse q polarization in a transversely polarized proton (“Collins effect”) [8]. This mechanism was considered to be suppressed for $p_\uparrow + p \rightarrow \pi + X$ until recently [9, 10]. Spin-correlated TMD distribution functions (“Sivers functions”) [11, 12] can explain large A_N [13]. These functions describe parton orbital motion within the proton, and so are important for understanding the structure of the proton.

Although Sivers functions are extracted from SIDIS results, there is no proof [14] that they factorize in pQCD calculations of $p_\uparrow + p \rightarrow \pi + X$. A factorized framework involving twist-3 qg correlators has been introduced [15] and has successfully described [16] previous A_N results [4, 6] for $p_\uparrow + p \rightarrow \pi + X$. Of relevance to both approaches is a transverse momentum (k_T) that is integrated over in inclusive processes. This k_T is intrinsic parton motion in the Sivers functions and its average is related to the inverse proton radius. Large k_T is where qg correlators are expected to provide a robust framework. Small k_T is where Sivers functions are expected to be applicable. Intermediate k_T values yield the same results in the two approaches, because moments of the Sivers functions are found to be related to the qg correlators [17, 18].

Both theoretical frameworks [13, 16] predict that A_N will increase as the longitudinal momentum (p_L) of the pion increases, usually given by Feynman- x , $x_F = 2p_L/\sqrt{s}$. Both frameworks predict that, at fixed x_F , A_N

will decrease with increasing transverse momentum (p_T), for $p_T > 1.2$ GeV/ c .

Analyzing powers in the hadroproduction of pions have been measured before, and typically show a strong increase as x_F increases [2, 3, 4, 5, 6]. Virtually no previous experimental results exist for the dependence of A_N on p_T at fixed x_F . For $\sqrt{s} \leq 20$ GeV, the cross sections are at least ten times larger than pQCD calculations for x_F values where A_N is sizeable [19]. This led to the suggestion that beam fragmentation, the dissociation of the polarized proton by the unpolarized target, was responsible for the spin effects, and the expectation that at sufficiently large p_T these spin effects would vanish. At $\sqrt{s}=200$ GeV, inclusive π cross sections at central and forward rapidity are found to be in agreement with pQCD calculations above $p_T \sim 2$ GeV/ c , and are included with world data for π production from e^+e^- collisions, SIDIS, and other $p+p$ collider results in a global analysis of fragmentation functions [20]. A_N that increase with x_F are found at $\sqrt{s} = 200$ GeV [6, 21, 22], but both precision measurements and the determination of the dependence on p_T have, until now, been missing.

In this Letter, we report precision measurements of the x_F dependence and first measurements of the p_T dependence of A_N at fixed x_F for $p_\uparrow + p \rightarrow \pi^0 + X$ at $\sqrt{s} = 200$ GeV. The experiment has been performed at the Solenoidal Tracker at RHIC (STAR) [23] at the Relativistic Heavy Ion Collider (RHIC) at Brookhaven National Laboratory. The experiment was performed using vertically polarized colliding beams. Asymmetries are formed from yields measured with left-right symmetrical detectors, tagged by the polarization direction of one beam and summing over the polarization of the other beam. Positive x_F is probed by considering polarization of the beam heading towards the detectors and negative x_F is probed by considering polarization of the beam heading away from the detectors.

Measurements were carried out with a modular electromagnetic calorimeter, known as the Forward Pion Detector (FPD), positioned at large pseudorapidity ($\eta = -\ln(\tan\theta/2)$). The $\langle\eta\rangle=4.0$ results, and some $\langle\eta\rangle=3.7$ results, reported here were obtained in the 2003 (2005) run having integrated luminosity $L_{int}=0.25$ pb $^{-1}$ (0.1 pb $^{-1}$) and average beam polarization $P_b \sim 35\%$ (50%). $\langle\eta\rangle=3.3$ and most of the $\langle\eta\rangle=3.7$ measurements were performed in the 2006 run, which resulted in $L_{int}=6.8$ pb $^{-1}$ with $P_b \sim 55\%$. In the 2006 run, 111 of the 120 possible bunches of both RHIC rings, called “Blue” and “Yellow”, were filled with protons having predetermined patterns of polarization signs. The unfilled 9 bunches are sequential and correspond to the abort gap needed to eject the

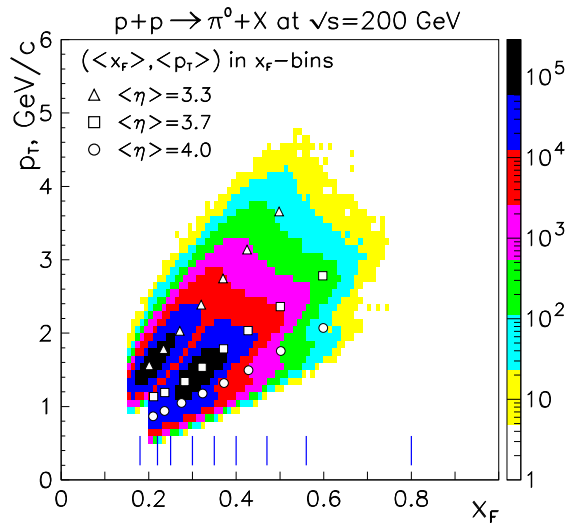


FIG. 1: Correlation between pion longitudinal momentum scaled by $\sqrt{s}/2$ (x_F) and transverse momentum (p_T) for all events. Bins in x_F used in Figs. 2 and 4 are indicated by the vertical lines. There is a strong correlation between x_F and p_T at a single pseudorapidity ($\langle \eta \rangle$).

stored beams. P_b was measured every 3 hours during RHIC stores by a polarimeter that detected recoil carbon ions produced in elastic scattering of protons from carbon ribbon targets inserted into the beams. The effective A_N of this polarimeter was determined from $p_{\uparrow} + p_{\downarrow}$ elastic scattering from a polarized gas jet target [24] thereby determining $P_b = 55.0 \pm 2.6\%$ ($56.0 \pm 2.6\%$) for the Blue (Yellow) beam in the 2006 run [25].

The FPD comprises four modules, each containing a matrix of lead glass (PbGl) cells of dimension $3.8 \text{ cm} \times 3.8 \text{ cm} \times 18$ radiation lengths. Pairs of modules were positioned symmetrically left (L) and right (R) of the beamline in both directions, at a distance of ~ 750 cm from the interaction point [21]. The modules facing the Yellow (Blue) beam are square matrices of 7×7 (6×6) PbGl cells. Data from all FPD cells were encoded for each bunch crossing, but only recorded when the summed energy from any module crossed a preset threshold.

Neutral pions are reconstructed via the decay $\pi^0 \rightarrow \gamma\gamma$. The offline event analysis included conversion of the data to energy for each cell, formation of clusters and reconstruction of photons using a fit with the function that parameterizes the average transverse profile of electromagnetic showers. Collision events were identified by requiring a coincidence between the east and west STAR beam-beam counters (BBC), as used for cross section measurements [27]. Events were selected when two reconstructed photons were contained in a fiducial volume, whose boundary excludes a region of width $1/2$ cell at the module edges. Detector calibration was determined from the π^0 peak position in di-photon invariant mass ($M_{\gamma\gamma}$) distributions. The estimated calibration accuracy

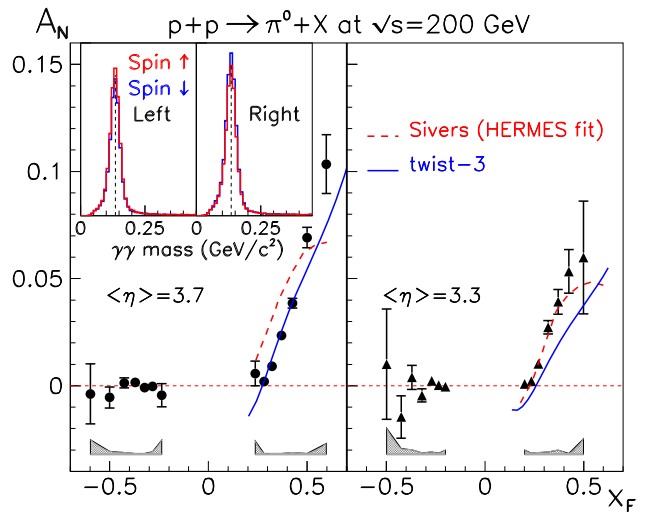


FIG. 2: Analyzing powers in x_F bins (see Fig. 1) at two different $\langle \eta \rangle$. Statistical errors are indicated for each point. Systematic errors are given by the shaded band, excluding normalization uncertainty. The calculations are described in the text. The inset shows examples of the spin-sorted invariant mass distributions. The vertical lines mark the π^0 mass.

is 2%. The analysis was validated by checking against full PYTHIA/GEANT simulations [26]. The reconstructed π^0 energy resolution is given by $\delta E_{\pi}/E_{\pi} \approx 0.16/\sqrt{E_{\pi}}$.

Due to the limited acceptance there is a strong correlation between x_F and p_T for reconstructed π^0 (Fig. 1). Spin effects in the x_F - p_T plane are studied by positioning the calorimeters at different transverse distances from the beam, maintaining L/R symmetry for pairs of modules. Fig. 1 shows loci from $\langle \eta \rangle = 3.3, 3.7$ and 4.0 . There is overlap between the loci, providing cross checks between the measurements. Because the measurements were made at a colliding beam facility both $x_F > 0$ and $x_F < 0$ results are obtained concurrently.

Events with $0.08 < M_{\gamma\gamma} < 0.19 \text{ GeV}/c^2$ were counted separately by spin state from one or the other beam, with no condition on the spin state of the second beam, in the x_F bins shown in Fig. 1. For each run i , $A_{N,i}$ for each bin was then determined by forming a cross ratio

$$A_{N,i} = \frac{1}{P_b} \frac{\sqrt{N_{L\uparrow,i}N_{R\downarrow,i}} - \sqrt{N_{L\downarrow,i}N_{R\uparrow,i}}}{\sqrt{N_{L\uparrow,i}N_{R\downarrow,i}} + \sqrt{N_{L\downarrow,i}N_{R\uparrow,i}}}, \quad (1)$$

where $N_{L(R)\uparrow(\downarrow),i}$ is the number of events in the L (R) module when the beam polarization was up (down). Equation (1) cancels spin dependent luminosity differences through second order. Statistical errors were approximated by $\Delta A_{N,i} = [P_b \sqrt{N_{L\uparrow,i} + N_{L\downarrow,i} + N_{R\uparrow,i} + N_{R\downarrow,i}}]^{-1}$, valid for small asymmetries. All measurements of P_b for a store were averaged and applied to get $A_{N,i}$ for each bin. The run-averaged $A_N \pm \Delta A_N$ values are shown in Fig. 2.

Systematic errors potentially arise from several sources. The bunch counter, used for the spin directions,

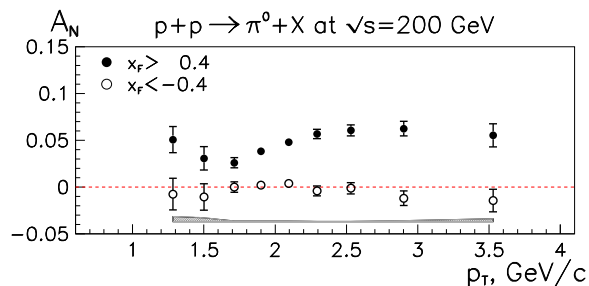


FIG. 3: Analyzing powers versus π^0 transverse momentum (p_T) for events with scaled π^0 longitudinal momentum $|x_F| > 0.4$. Errors are as described for Fig. 2.

identifies events in the abort gaps arising from single-beam backgrounds. They account for $< 5 \times 10^{-4}$ of the observed yield. Systematic effects from gain variations with time are controlled by polarization reversals of the stored beam bunches, as demonstrated by examples of spin-sorted $M_{\gamma\gamma}$ for L,R modules in the inset to Fig. 2. Distributions of the significance, $S_i = (A_{N,i} - A_N)/\Delta A_{N,i}$, are well described by zero mean value Gaussian distributions with σ equal to unity, as expected if the uncertainties are dominated by statistics, except near the trigger threshold where larger σ is observed. Systematic errors are estimated from $\sigma \times \Delta A_N$ and differences in A_N associated with π^0 identification, with the largest value chosen. The upper limit on a correlated systematic error, common to all points, arising from instrumental effects is $\delta A_N \approx 4 \times 10^{-4}$.

The same pair of modules concurrently measure A_N values consistent with zero for $x_F < 0$ and A_N that increases with x_F for $x_F > 0$, depending on which beam spin is chosen. Null results at $x_F < 0$ are natural since a possible gluon Siverts function is probed where the unpolarized gluon distribution is large. For $x_F > 0$, a calculation [13, 28] using quark Siverts functions fit [29] to SIDIS data [7] best describes our results at $\langle \eta \rangle = 3.3$. Twist-3 calculations [16] that fit $p_\uparrow + p \rightarrow \pi + X$ data at $\sqrt{s} = 20$ GeV [4] and preliminary RHIC results from the 2003 and 2005 runs at $\sqrt{s} = 200$ GeV [21, 22] best describe the data at $\langle \eta \rangle = 3.7$. Both calculations are in fair agreement with the variation of A_N with x_F . Neither calculation describes data at both $\langle \eta \rangle$.

Events from modules at different $\langle \eta \rangle$ that overlap in the x_F - p_T plane (Fig. 1) provide consistent results. Hence, it is possible to further bin the results not only by x_F but also by p_T . For this analysis, p_T is determined from the measured energy, the fitted position of the π^0 within an FPD module, and the measured position of the module relative to the beam pipe and to the collision vertex. The z component of the event vertex uses a coarse time difference between the east and west BBC, and is determined to ~ 20 cm resulting in $\Delta p_T/p_T = 0.04$, where Δp_T is the uncertainty in p_T . One method of determining the p_T

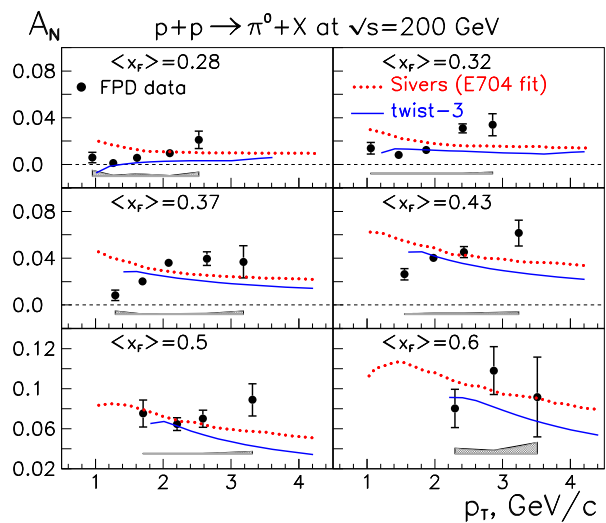


FIG. 4: Analyzing powers versus π^0 transverse momentum (p_T) in fixed x_F bins (see Fig. 1). Errors are as described for Fig. 2. The calculations are described in the text.

dependence (Fig. 3) was to select events with $|x_F| > 0.4$. A_N is consistent with zero for $x_F < -0.4$. For $x_F > 0.4$, there is a hint of an initial decrease of A_N with p_T , although the statistical errors are large, since $\langle \eta \rangle = 4.0$ data were only obtained in the 2003 and 2005 runs with limited integrated luminosity and polarization. For $p_T > 1.7$ GeV/c, A_N tends to increase with p_T for $x_F > 0.4$. This is contrary to the theoretical expectation that A_N decreases with p_T .

The results in Fig. 3 may still reflect small correlations between x_F and p_T for each point, rather than the dependence of A_N on p_T at fixed x_F . To eliminate this correlation, event selection from Fig. 1 was made in bins of x_F , followed by bins in p_T . The resulting variation of A_N with p_T is shown in Fig. 4, compared to calculations [13] using a Siverts function fit to $p_\uparrow + p \rightarrow \pi + X$ data [4] and twist-3 calculations [16]. For each point, the variation of $\langle x_F \rangle$ is smaller than 0.01. There is a clear tendency for A_N to increase with p_T , and no significant evidence over the measured range for A_N to decrease with increasing p_T , as expected by the calculations. This discrepancy may arise from unexpected TMD fragmentation contributions, x_F, p_T dependence of the requisite color-charge interactions, evolution of the Siverts functions, or from process dependence not accounted for by the theory.

In summary, we have measured the x_F and p_T dependence of the analyzing power for forward π^0 production in $p_\uparrow + p$ collisions at $\sqrt{s} = 200$ GeV in kinematics ($0.3 < x_F < 0.6$ and $1.2 < p_T < 4.0$ GeV/c) that straddle the region where cross sections are found in agreement with pQCD calculations. The x_F dependence of the π^0 A_N is in fair agreement with both a collinear twist-3 calculation and a calculation assuming factorization that attributes the spin effects to spin-correlated in-

trinsic transverse momentum of the quarks within the proton. Recent theoretical work interrelates these descriptions. Both calculations expect the spin effects to monotonically decrease with increasing p_T for $p_T > 1.2$ GeV/c. Measurements of the p_T dependence at fixed x_F of A_N are not consistent with these expectations. This may reflect the presence of additional mechanisms for these spin effects. Future measurements capable of disentangling TMD fragmentation and distribution function contributions to π^0 spin effects, and measurements of A_N for real and virtual photon production sensitive to only Sivers contributions, are required to definitively establish if partonic orbital motion is the correct explanation of these effects.

We thank the RHIC Operations Group and RCF at BNL, and the NERSC Center at LBNL and the resources provided by the Open Science Grid consortium for their support. This work was supported in part by the Offices of NP and HEP within the U.S. DOE Office of Science; the U.S. NSF; a sponsored research grant from Renaissance Technologies Corporation; the BMBF of Germany; CNRS/IN2P3, RA, RPL, and EMN of France; EPSRC of the United Kingdom; FAPESP of Brazil; the Russian Ministry of Sci. and Tech.; the Ministry of Education and the NNSFC of China; IRP and GA of the Czech Republic, FOM of the Netherlands, DAE, DST, and CSIR of the Government of India; Swiss NSF; the Polish State Committee for Scientific Research; Slovak Research and Development Agency, and the Korea Sci. & Eng. Foundation.

* URL: www.star.bnl.gov

- [1] G. L. Kane, J. Pumplin, W. Repko, Phys. Rev. Lett. **41**, 1689 (1978).
 [2] R. D. Klem *et al.*, Phys. Rev. Lett. **36**, 929 (1976); W. H. Dragoset *et al.*, Phys. Rev. D **18**, 3939 (1978).
 [3] S. Saroff *et al.*, Phys. Rev. Lett. **64**, 995 (1990); B. E. Bonner *et al.*, Phys. Rev. D **41**, 13 (1990).
 [4] B. E. Bonner *et al.*, Phys. Rev. Lett. **61**, 1918 (1988); A. Bravar *et al.*, *ibid.* **77**, 2626 (1996); D. L. Adams *et al.*, Phys. Lett. B **261**, 201 (1991); **264**, 462 (1991); Z. Phys. C **56**, 181 (1992).
 [5] K. Krueger *et al.*, Phys. Lett. B **459**, 412 (1999); C. E. Allgower *et al.*, Phys. Rev. D **65**, 092008 (2002).
 [6] J. Adams *et al.*, Phys. Rev. Lett. **92**, 171801 (2004).
 [7] A. Airapetian *et al.*, Phys. Rev. Lett. **94**, 012002 (2005).
 [8] J. Collins, Nucl. Phys. B **396**, 161 (1993).
 [9] M. Anselmino *et al.*, Phys. Rev. D **71**, 014002 (2005).
 [10] F. Yuan, Phys. Lett. B **666**, 44 (2008).
 [11] D. Sivers, Phys. Rev. D **41**, 83 (1990); **43**, 261 (1991).
 [12] S. J. Brodsky, D. S. Hwang, I. Schmidt, Phys. Lett. B **530**, 99 (2002).
 [13] U. D'Alesio, F. Murgia, Phys. Rev. D **70**, 074009 (2004).
 [14] J. Collins, J. Qiu, Phys. Rev. D **75**, 114014 (2007).
 [15] J. Qiu, G. Sterman, Phys. Rev. D **59**, 014004 (1998).
 [16] C. Kouvaris, J. Qiu, W. Vogelsang, F. Yuan, Phys. Rev. D **74**, 114013 (2006).
 [17] D. Boer, P. J. Mulders, P. Pijlman, Nucl. Phys. B **667**, 201 (2003).
 [18] X. Ji, J. Qiu, W. Vogelsang, F. Yuan, Phys. Rev. Lett. **97**, 082002 (2006).
 [19] C. Bourrely, J. Soffer, Eur. Phys. Journ. C **36**, 371 (2004).
 [20] D. de Florian, R. Sassot, M. Stratmann, Phys. Rev. D **75**, 114010 (2007).
 [21] L. C. Bland, arXiv:hep-ex/0602012.
 [22] F. Videbaek (BRAHMS), AIP Conf. Proc. **792**, 993 (2005).
 [23] K. H. Ackermann *et al.*, Nucl. Instr. Meth. A **499**, 624 (2003).
 [24] H. Okada *et al.*, Phys. Lett. B **638**, 450 (2006).
 [25] A. Bazilevsky *et al.*, RHIC/CAD Accelerator Physics Note 298 (2007).
 [26] T. Sjöstrand *et al.*, Comp. Phys. Commun. **135**, 238 (2001). GEANT 3.21, CERN program library.
 [27] J. Adams *et al.*, Phys. Rev. Lett. **97**, 152302 (2006).
 [28] M. Boglione, U. D'Alesio, F. Murgia, Phys. Rev. D **77**, 051502 (2008).
 [29] M. Anselmino *et al.*, Phys. Rev. D **72**, 094007 (2005).